

<https://doi.org/10.1016/j.apenergy.2021.117006>

Access to this work was provided by the University of Maryland, Baltimore County (UMBC) ScholarWorks@UMBC digital repository on the Maryland Shared Open Access (MD-SOAR) platform.

Please provide feedback

Please support the ScholarWorks@UMBC repository by emailing scholarworks-group@umbc.edu and telling us what having access to this work means to you and why it's important to you. Thank you.

High Performance Scalable and Cost-Effective Thermoelectric Devices Fabricated Using Energy Efficient Methods and Naturally Occuring Materials

Eunhwa Jang¹, Priyanshu Banerjee¹, Jiyuan Huang¹, Deepa Madan^{1*}

Department of Mechanical Engineering, University of Maryland, Baltimore County, 1000 Hilltop Circle, Baltimore, MD 21250, USA

* Correspondence: deemadan@umbc.edu; Tel.: +1-410-455-3307

Highlights

- Fabricated a thermoelectric generator device using a stencil printing method
- Developed an, energy-efficient process using novel binder, mixed particles size, and hot pressing
- Used naturally occurring chitosan gel electrolyte and Bi as thermoelectric material
- The device achieved a power output of 73 μW and a power density of 566 $\mu\text{W}/\text{cm}^2$

Abstract

Various printing methods have recently been employed to manufacture thermoelectric generators. While providing a scalable alternative to manufacturing thermoelectric generators, these printing techniques consume excessive energy by using long-duration and high-temperature sintering to reduce the interfacial connections and grain boundaries between thermoelectric particles. We report an inexpensive and energy-saving technique for fabricating thermoelectric generator devices that can be employed for low-waste heat applications. This technique involves a synergistic approach, using a small amount of binder (0.05 wt.%), a heterogenous distribution of thermoelectric particles of varying size, low temperature (120 °C) and short duration (30 min) curing, and application of uniaxial mechanical pressure (200 MPa) to reduce the grain boundaries and interfacial connection and to enhance electrical conductivity of thermoelectric composite films and thermoelements. In this work, we present a thermoelectric prototype fabricated on gold-coated Kevlar substrate using p-type chitosan-100 mesh $\text{Bi}_{0.5}\text{Sb}_{1.5}\text{Te}_3$ and n-type chitosan-100 mesh Bi composite inks. The dimension of a single thermoelement was 6.5 mm \times 2.3 mm \times 150 μm . The 9-couple planar device was able to produce a power output of 73 μW at a voltage of 26 mV, and at a current of 2.8 mA at a temperature difference of 40 K, which is sufficient to power wireless sensor devices. Using energy-efficient methods and naturally occurring materials (Bi and chitosan), this device achieved a power density of 566 $\mu\text{W}/\text{cm}^2$ for a temperature difference of 40 K matching the best reported power densities of printed thermoelectric devices fabricated using high temperature and long duration.

Keywords: Printable Thermoelectric Generators, Energy-efficient, Scalable, Cost-effective, Naturally Occurring Chitosan, Bi

1. Introduction

The exponential growth in the market for wearable devices and Internet of Things (IOT) demands long lasting, uninterrupted power for the wireless sensor networks (WSN) used in these applications [1,2]. The main power resource for WSNs is primary batteries which require frequent

replacement. Battery replacement is a labor-intensive, wasteful process which greatly limits the WSN efficiency and deployment in remote locations. Therefore, a long-lasting and environmentally friendly power supply alternative is desired for future WSN applications. Compared to solar or piezoelectric devices, which are dependent on sun or mechanical motion, thermoelectric generators (TEGs) are a viable choice which can generate electricity by scavenging the waste heat from body or ambient waste heat [3,4].

The performance of TEG device depends on the thermoelectric (TE) properties (electrical conductivity, Seebeck coefficient, and thermal conductivity) of the TE materials (also known as ZT) and on the TEG device design (device dimensions and number of thermoelements). Efficient TE materials should have high electrical conductivity, high Seebeck coefficient and low thermal conductivity. The high electrical conductivity of TE materials provides high current, the high Seebeck coefficient provides high voltage, and low thermal conductivity provides a high temperature difference across the TEG device. The high aspect ratio (length to width ratio) of the TEG device plays an important role in maintaining a high temperature difference across the device, which will thereby result in a high voltage output [5]. Similarly, if a high number of n- and p-type thermoelements (together known as couples) can be packed in a small area of the TEG device, it will also result in high voltage and high-power output. Therefore, to obtain the high power output of the TEG device, we should use materials with high ZT, high aspect ratio (length to width ratio) of thermoelements, and a large number of couples [6,7].

The traditional rigid TEGs have many inevitable weaknesses, despite the fact that they are made using thermoelectric bulk materials having ZT of 1 at room temperature, permitting them to achieve high-power output. From a manufacturing perspective, the pick and place methods used to manufacture these TEGs is extremely labor-intensive, and the high-temperature annealing or sintering processes are energy-intensive. Similarly, from the design perspective, traditional TEGs are rigid and have a very low aspect ratio (bulk TE materials are brittle, making it difficult to obtain a high aspect ratio) while consisting of low-density arrays. Therefore, an alternative approach to energy-efficient, scalable, cost-effective, high-performing TEGs would be required to meet the power supply demands for WSN used in the wearable devices and IoT market.

Additive manufacturing techniques have proved promising in addressing the pitfalls of traditionally manufactured TEGs [8–10]. This technology uses an automatic printer to deposit thermoelectric composite ink onto the substrates while minimizing the labor effort and the materials waste from dicing the bulk materials to obtain thermoelements. Additionally, this technique has superior flexibility in obtaining a high aspect ratio of TEG devices and a high number of couples [8]. Although printing techniques have many advantages, printed TEGs perform poorly compared with TEGs made from bulk materials [11]. Unlike bulk materials, the printing method requires thermoelectric materials to be in a special ink form, which is synthesized using micro-size or nano-size TE particles combined with a high amount of insulating binder [12–14]. Because of the low electrical conductivity of the binder, the thermoelectric performance of TE films is negatively affected, reducing the overall performance of the TEGs. Moreover, the micro- or nano-sized TE particles have poor interfacial connections with the polymer binder, while the presence of numerous grain boundaries in TE composite films also adversely affects their electrical conductivity. Evans et al. employed dispenser printing to print both epoxy-based n-type and p-type TE composite films, but their overall electrical conductivity was about two orders of magnitude lower than that of bulk materials [15–17].

Many groups have made progress in improving the thermoelectric performance of printed TEGs in the past few years. Cho et al. used a post-annealing process with a removable binder and mechanical pressing to achieve a power density of 7.34 mW/cm^2 at a temperature difference (ΔT) of 28 K for their 200-couple TEG prototype [9]. Zhang et al., on the other hand, directly used extra Te together with p-type BST and removable binder to improve the electrical conductivity of their 4-couple TEG prototype, thus achieving a power density of 18.8 mW/cm^2 at a ΔT of 80 K [18]. Cao et al. used an epoxy binder system along with cold pressing to reduce the resistivity of their 8-couple TEG prototype, ultimately generating a maximum power of 40.3 nW at a ΔT of 20 K [19]. Although these groups were able to overcome some of the obstacles related to low thermoelectric performance discussed above, the challenge remains how to make TEG cost effective using energy-efficient methods and naturally available materials. Both Cho's and Zhang's groups used a combination of removable binder, high-temperature sintering (450°C for 1-3 hrs.), and mechanical pressing to improve the electrical conductivity of the TEG device. However, these processes were extremely energy-intensive, with curing temperatures reaching up to 500°C and curing times reaching 3-6 hours to enhance the electrical conductivity of the films/devices [18–22].

In this work, we propose to use an energy-efficient method and naturally occurring materials (Bi and chitosan) to fabricate cost-effective and scalable TEG devices while overcoming the challenges of the energy-intensive processes reported by previous researchers [9–11]. To fabricate efficient TEG devices we need n- and p-type TE materials; therefore, we are using commercially available 100 mesh p-type $\text{Bi}_{0.5}\text{Sb}_{1.5}\text{Te}_3$ (BST) particles and naturally available 100 mesh n-type Bismuth (Bi) particles to fabricate the thermo elements of TEG. The thermoelectric n- and p-type composite inks were synthesized using n- and p-type TE particles and naturally occurring chitosan binder. Chitosan has exceptionally good adhesive properties, which makes it a better candidate than epoxy and removable binder. Unlike the traditional binder (e.g. epoxy), which needs about 5-25 wt. % to effectively bind all TE particles, the chitosan binder needs less than 1 wt. % to achieve the same effect [23–26]. Additionally, the 0.05 wt. % of chitosan binder is too small to have any significant impact on the electrical conductivity of the thermoelectric composite film. Also, removable and epoxy binders require high temperature and long duration (energy intensive process) to decompose and sinter the particles, as compared to the chitosan binder which does not need to be removed from the film, making it energy-efficient and cost-effective. We also used heterogeneous-sized particles for our thermoelectric materials because, during the fabrication process, smaller particles can fill the voids between larger particles, thereby enhancing the inter-connections and forming longer continuous paths. This enabled the charge carriers to flow smoothly without getting scattered. Finally, hot pressing (120°C , 30 minutes, 200 MPa) resulted in a bulk-like structure, which means the films were compact and dense and had fewer grain boundaries. The synergetic effects of using a small amount of naturally occurring binder, heterogeneous distribution of TE particles of varying sizes, hot pressing, and low temperature and short duration helped to achieve an electrical conductivity and ZT similar to the previously reported printed TEG films, without an energy-intensive curing method [27–29].

We successfully fabricated a 9-couple TEG prototype device using p-type BST-chitosan and n-type Bi-chitosan as the two thermoelements to make one couple. The highest power output of 73 μW was achieved at a temperature difference (ΔT) of 40 K for which the voltage of the TEG prototype was 26 mV and the current was 2.8 mA. Using the aforementioned energy-efficient fabrication method, this prototype achieved a power density of $566 \mu\text{W/cm}^2$ at ΔT of 40 K. This is one of the best reported values of power and power densities among other printed TEG devices

fabricated using energy-intensive (high temperature and long duration) curing methods. This power output is sufficient to power various WSN applications used in various Internet of Things (IOT) applications

2. Experimental Method

We used previously developed p-type chitosan-100 mesh BST (1:2000 wt. ratio) and n-type chitosan-100 mesh Bi (1:2000 wt. ratio) inks [30,31]. Using these p- and n-type inks, we stencil printed p- and n-type films (thickness 150 μm , area 7mm x 7mm) and hot pressed them at a temperature of 120°C for 30 minutes at 200 MPa applied pressure. Since the TEG device that we developed is intended for low waste heat applications (up to 100°C), we carried out high-temperature (25°C, 50°C, 75°C, and 100°C) electrical conductivity and Seebeck coefficient measurements for n- and p-type composite films. The in-plane room-temperature and high-temperature electrical conductivity was measured using a Hall effect measurement system (Ecopia HMS-3000) together with a heating controller (HMS-3300) to increase the temperature up to 100 °C. For the Seebeck coefficient measurement, a custom setup was used to measure the Seebeck coefficient at room temperature and high temperature (50 °C, 75 °C, and 100 °C) The details of custom built Seebeck measurements system were described in our previous publications [30,31]. The Thermal conductivity of the p-type chitosan-BST composite film was measured using TCi thermal conductivity [31]. The thermal conductivity of chitosan-Bi composite film was measured using the optical pump-probe technique steady-state thermoreflectance as described in our previous publication [30].

2.1 Thermoelectric generator (TEG) prototype fabrication

For the TEG device fabrication, gold-coated Cu electrode was first deposited on the Kevlar substrate to avoid the high contact resistance between Kevlar substrates. This was followed by stencil printing of n- and p-type thermoelements on the Kevlar substrate. The gold-coated Cu electrodes (70 μm Cu, 5 μm Ni, 0.03 μm Au) were fabricated in South Korea (PASF250, Sueco Advanced Material Co., Ltd.) on Kevlar substrates using a customized device pattern provided by us. On top of the gold electrodes, we stencil printed solder paste (130 μm thick) using stencil printing. The application of soldering paste was necessary to provide better adhesion between gold electrodes and thermoelements as well as avoid delamination of thermoelements after hot pressing. Commercially available solder paste (DS-0201LF58) was purchased from a Korean company (Danyang SOLTEC.) and stencil printed on the gold electrodes using stencil mask. The resistivity of solder paste is $2.4 \times 10^{-8} \Omega\text{-m}$. This was followed by stencil printing of p-type chitosan-100 mesh BST (1:2000 wt. ratio) and n-type chitosan-100 mesh Bi (1:2000 wt. ratio) TE inks on the substrate to form p- and n-type thermoelements respectively. The dimensions of each thermoelement was 6.5 mm (L) x 2.3 mm (W) x 160 μm (T) while the spacing between two thermoelements was 2.5mm. The deposited thermoelements were cured at 120 °C in a vacuum oven to evaporate the solvent for 10 minutes followed by hot-pressing at 200 MPa at a temperature of 120 °C under nitrogen inert atmosphere for 30 minutes. The hot pressing acted a pivotal step to provide the compact and dense film morphology to enhance the TE films' electrical conductivity. Hot pressing also facilitated a good adhesion between thermoelements, soldering paste, and metal electrodes and reduced the overall contact resistance of the TEG device. Two Kapton films were placed on the top and bottom of the TEG device before hot-pressing to avoid any possible contamination on the surface of the thermo elements. Electrical connections were made using soldering paste and Cu electrical wires. The schematic for ink synthesis, TE film preparation, and fabrication of the TEG prototype is shown in Fig. 1. The actual image of TEG device is shown in Fig. 2.

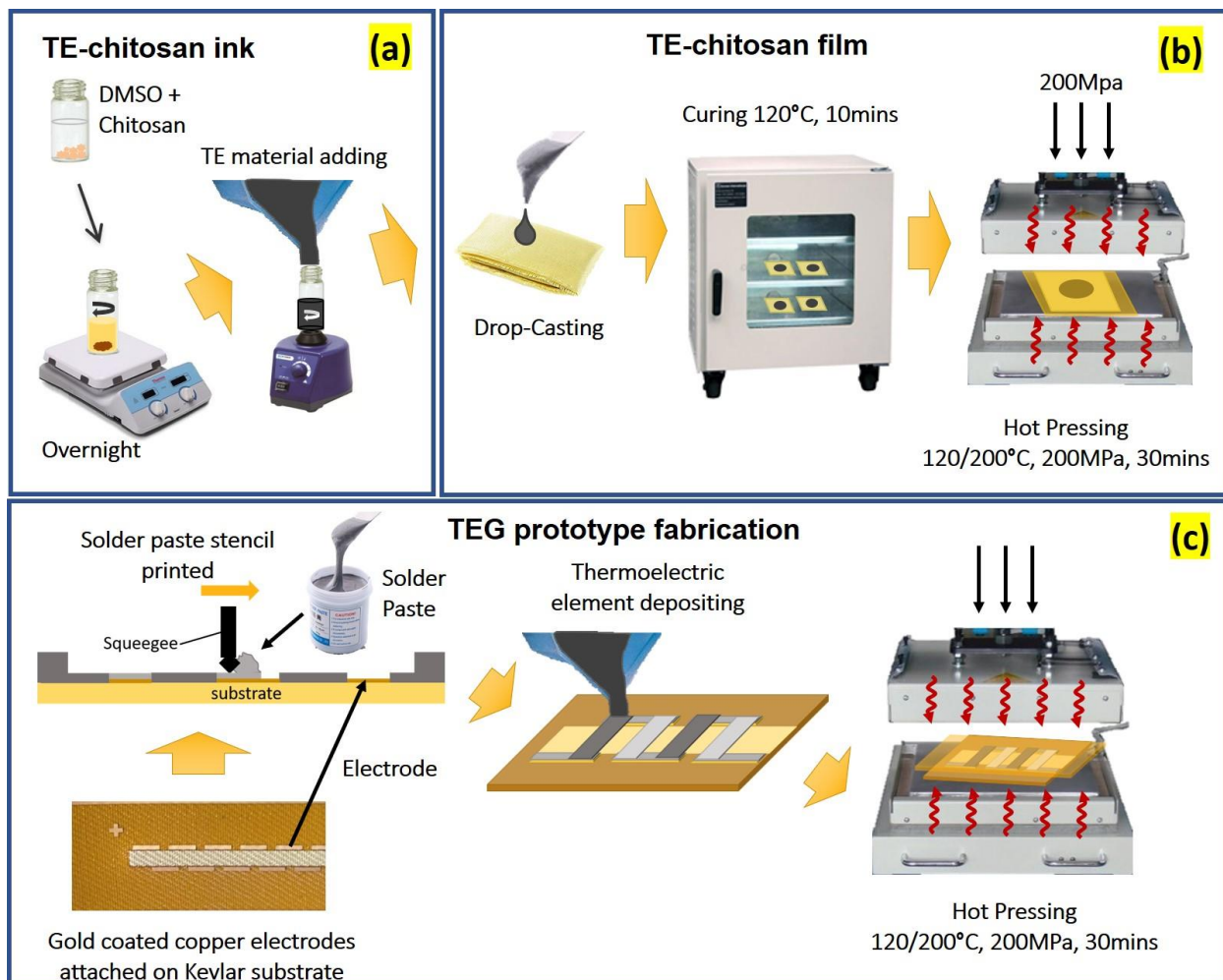


Fig. 1. Process schematic for (a) TE-chitosan ink (b) TE-chitosan film (c) TEG prototype fabrication



Fig. 2. Photo of the TEG prototype with scale

2.2 TEG prototype testing

The TEG open circuit voltage and power output characterization was measured at various temperature differences. To maintain a constant temperature difference across the device, the temperature differences were generated using a silicon heater strip for the hot side and peltiers for the cold side. A DC power source was used to supply sufficient voltage to the silicon heater strip to maintain the desired temperature on the hot-side. Another DC power source was used to supply the voltage to the peltiers to maintain the desired cold side temperature. Additionally, on the cold side a water-cooler heat sink was used to maintain the cold side temperature by adopting

a continuous flow of cold water. One end of the TEG prototype was mounted on top of the hot silicon strip heater, while the other end was mounted on the cold peltiers. Two thermocouples were connected on each end of the hot and cold side of the TEG device, while the other end was connected to two PID controllers. The two PID controllers were used to read the temperature of both the hot and cold sides of the TEG device. The TEG prototype was connected electrically in series with an external variable resistor and the output voltage was measured by a Keithley Source meter 2410-C. The open circuit voltage was measured by using 10 M Ω external load. The output voltage of the TEG prototype was measured by varying the load resistance. Each voltage was measured 50 times and the average value was recorded to avoid calculation errors. The current and power were calculated based on the load resistance and voltage measured at various temperature differences.

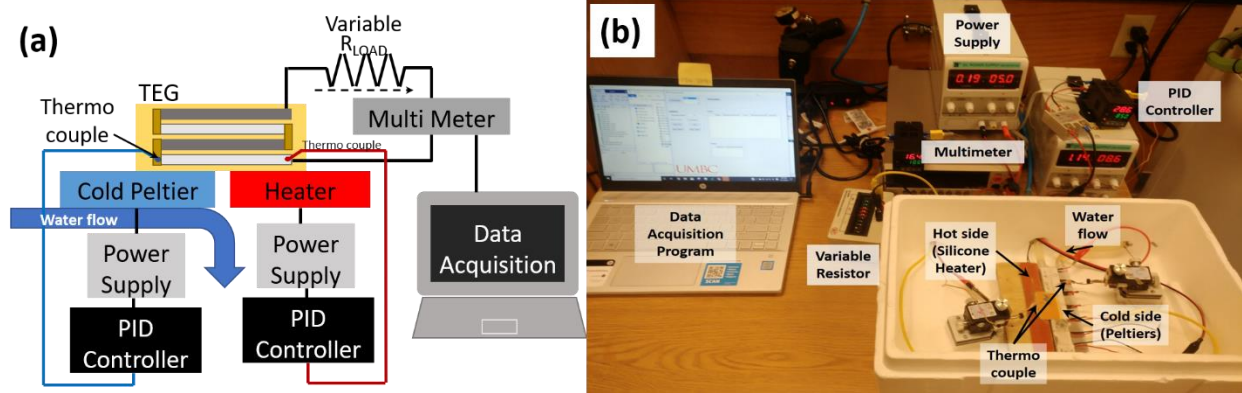


Fig. 3. (a) Schematic for TEG prototype device testing setup (b) Actual photo of the testing setup

3. Results and Discussions

3.1 Thermoelectric properties characterization of composite films at high temperature

The electrical conductivity and Seebeck coefficient of p-type chitosan 100 mesh BST and n-type chitosan Bi composite films (1:2000 weight ratio, hot pressed at 200 MPa) were measured at four different temperatures: 25 °C, 50 °C, 75 °C, and 100 °C. This was primarily done to observe how temperature and Seebeck coefficient affect the electrical conductivity of n- and p-type composite films prepared using hot pressing at 120°C for 30 minutes. By measuring these properties up to 100°C, it will help us to predict the stability and behavior of TEG devices fabricated using n- and p-type composite inks when the surrounding temperature is higher than room temperature. Fig. 4 shows the in-plane measurements of electrical conductivity and Seebeck coefficient for p-type chitosan-100 mesh BST and n-type chitosan-100 mesh Bi composite films. From Fig. 4a and 4b, we can see that the electrical conductivity and the Seebeck coefficient for the chitosan-BST composite films do not change significantly with increasing temperature.

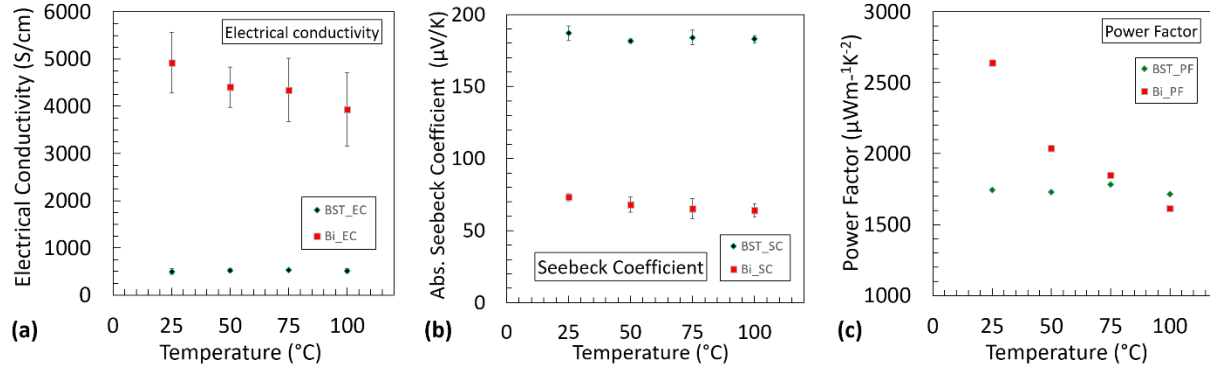


Fig. 4. (a) Electrical conductivity (b) Seebeck coefficient (c) Power Factor of p-type chitosan 100-mesh BST films and n-type chitosan-100 mesh Bi films (1:2000 wt. ratio, hot pressed at 200 MPa at 120 °C for 30 minutes) at 25 °C, 50 °C, 75 °C, and 100 °C

The electrical conductivity is in the range of 500-530 S/cm, which is lower than bulk BST electrical conductivity of 1200 S/cm due to the presence of insulating binder and the grain boundaries of thermoelectric particles [32]. However, it is worth mentioning that using a heterogenous particle size distribution (100 mesh), a small amount of insulating chitosan binder (0.05 wt. %), and hot pressing the TE composite films at 120°C for 30 minutes (energy efficient method) helped us to achieve an electrical conductivity value which is comparable to what other printed TE composite films achieved using energy-intensive processes that include high-temperature (up to 500°C) and long-duration (2-12 hrs.) curing [28,29]. To understand the electrical conductivity improvement in p-type composite films, we also performed SEM analysis. The SEM images of chitosan-BST composite film shown in Fig. 5(a) confirm that heterogenous particles packed well, resulting in dense structures with larger grains, better connections, and fewer grain boundaries and voids—similar to what we have shown in our previous publication of BTS-chitosan composite film due to cold pressing[31]. Larger grains and fewer grain boundaries resulted in high electrical conductivity of p-type composite films. The Seebeck coefficient of p-type composite films was in the range of 175-185 $\mu\text{V/K}$, similar to the Seebeck coefficient of bulk BST and printed BST composite films [27,28,32]. The similarity in the results of EC and SC yielded a power Factor (PF) ranged from 1730-1780 $\mu\text{W/mK}^2$ and did not vary much with varying temperature, as seen in Fig. 4c. These results are also comparable to the those reported in the literature on printed TE-composite films [12,17,29]. The thermal conductivity of the chitosan-100 mesh BST composite film was 0.62 W/m-K at room temperature and therefore ZT was 0.85 which is comparable to best reported values in literature [27,28].

The electrical conductivity of Bi chitosan composite film is seen to gradually decrease with increasing temperature, as shown in Fig 4a. The electrical conductivity of Bi chitosan composite films at room temperature was about 5000 S/cm, which is two-thirds of the electrical conductivity value of bulk Bi (8333 S/cm) [33]. The presence of an insulating chitosan binder in Bi composite films explains the lower electrical conductivity of the Bi-chitosan composite film as compared to bulk Bi. However, the electrical conductivity of chitosan-100 mesh Bi composite films (1:2000 wt ratio) is one order of magnitude greater than the previously reported Bi epoxy composite films [34]. To understand the improvement in chitosan Bi composite films, we performed SEM analysis; the corresponding SEM image is shown in Fig. 5(b). The image of Bi chitosan composite film shows a heterogenous particle size distribution of Bi (100 mesh), small amount of binder (0.05 wt. %) and hot pressing at 120 °C. All of these factors combined to achieve a bulk- like, compact,

and dense structure for the Bi-chitosan composite film. This bulk-like structure was beneficial in achieving electrical conductivity of Bi composite film similar to bulk Bi (semi metals). These Bi films, therefore, behave like semi metal at high temperature. We observed that the electrical conductivity of Bi chitosan composite films decreased to 4000 S/cm when the temperature was increased to 100 °C. For semimetals at elevated temperatures, thermal vibrations in the atoms intensify, leading to an increase in the scattering of charge carriers. This scattering of charge carriers causes the mean free path of the electrons to decrease, thereby reducing the mobility of electrons. This leads to a decrease in the overall electrical conductivity of the metals/semimetals at high temperature, which explains the gradual decrease in electrical conductivity of Bi chitosan composite films when the temperature is increased. Thus, the overall electrical conductivity of the Bi-chitosan composite film decreases with increasing temperature. The Seebeck coefficient of Bi chitosan composite films did not change much with increasing temperature and was in the range of -65 to -72 $\mu\text{V/K}$. The decrease in electrical conductivity with increasing temperature affects the power factor of the n-type composite films in a similar manner. Therefore, from Fig. 4 (c) it is evident that the power factor also decreases as the temperature increases for n-type Bi-chitosan composite films. The measured thermal conductivity of Bi-chitosan composite films was 4.4 W/m-K at room temperature and therefore ZT was 0.18.

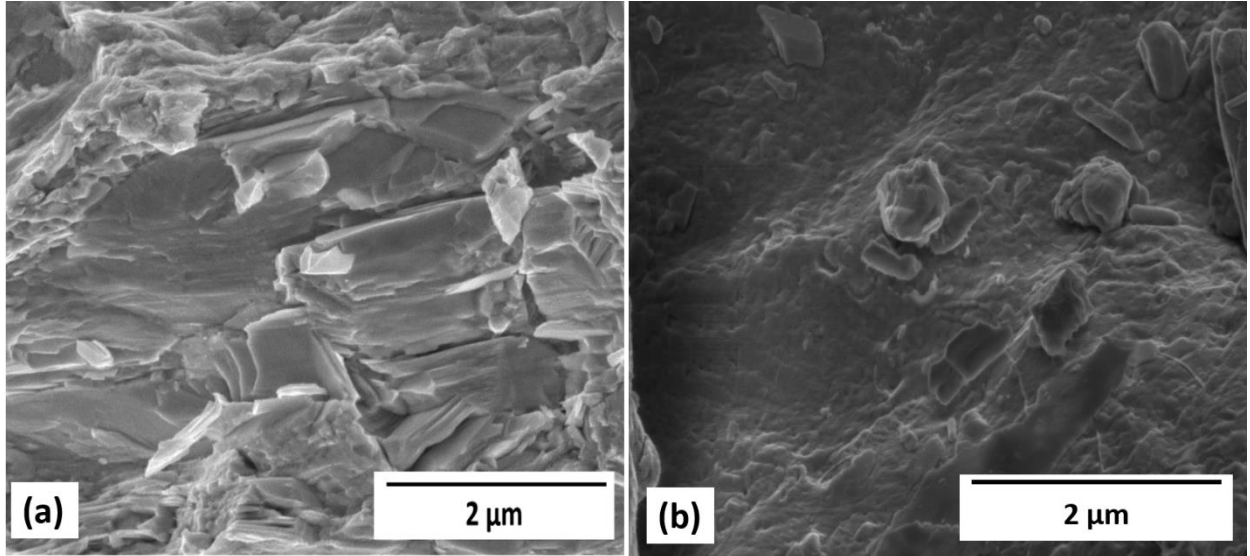


Fig. 5. Cross-sectional SEM image for (a) chitosan-100 mesh BST(1:2000 wt ratio) (b) chitosan-100 mesh Bi composite films (1:2000 wt ratio), hot pressing at 120 °C for 30 min.

3.2 TEG prototype device characterization

The open circuit voltage of 9 couple TEG device was measured at various temperature differences (8.5 K, 10 K, 15 K, 20 K, 26 K, 32 K, and 40 K). Fig. 6 shows the measured open circuit voltage of the TEG prototype and the calculated ideal open circuit voltage values based on the measured Seebeck coefficient values of n- and p-type TE composite films as a function of various temperature differences between 8.5 K to 40 K. The ideal open circuit voltage of a TEG can be written as

$$V_{oc} = m(\alpha_n + \alpha_p)\Delta T \quad (1)$$

where V_{OC} is the open circuit voltage, m is the number of n- and p-type thermoelement couples, α_n is the Seebeck coefficient of n-type thermoelectric material, α_p is the Seebeck coefficient of the p-type thermoelectric material, and ΔT is the temperature difference between the hot and cold side of the TEG. The Seebeck coefficient of the n-type chitosan Bi composite film was $-65 \mu\text{V/K}$ and the p-type chitosan $\text{Bi}_{0.5}\text{Sb}_{1.5}\text{Te}_3$ -chitosan composite film was $175 \mu\text{V/K}$ as shown in Fig. 4(b). We are using absolute Seebeck coefficient values of n-type and p-type composite films for calculating open circuit voltages. In Fig. 6, the measured and ideal open circuit voltage vs ΔT graph shows that the voltage increases linearly as ΔT increases. The voltage output of TEG device is directly proportional to the applied ΔT as well as the number of thermoelectric couples (m). At lower ΔT , the measured V_{OC} and calculated ideal V_{OC} are close to each other. However, at high ΔT , the difference between measured V_{OC} of prototype device and calculated ideal model increases. At ΔT of 40 K, the measured V_{OC} value of the prototype was 54 mV whereas it was 85 mV for the ideal model. This increase in voltage difference between ideal model and measured V_{OC} of TEG prototype at higher ΔT is a result of an increase in temperature fluctuations (conduction and convection) which makes it difficult to actually maintain a constant high ΔT across the TEG device [5].

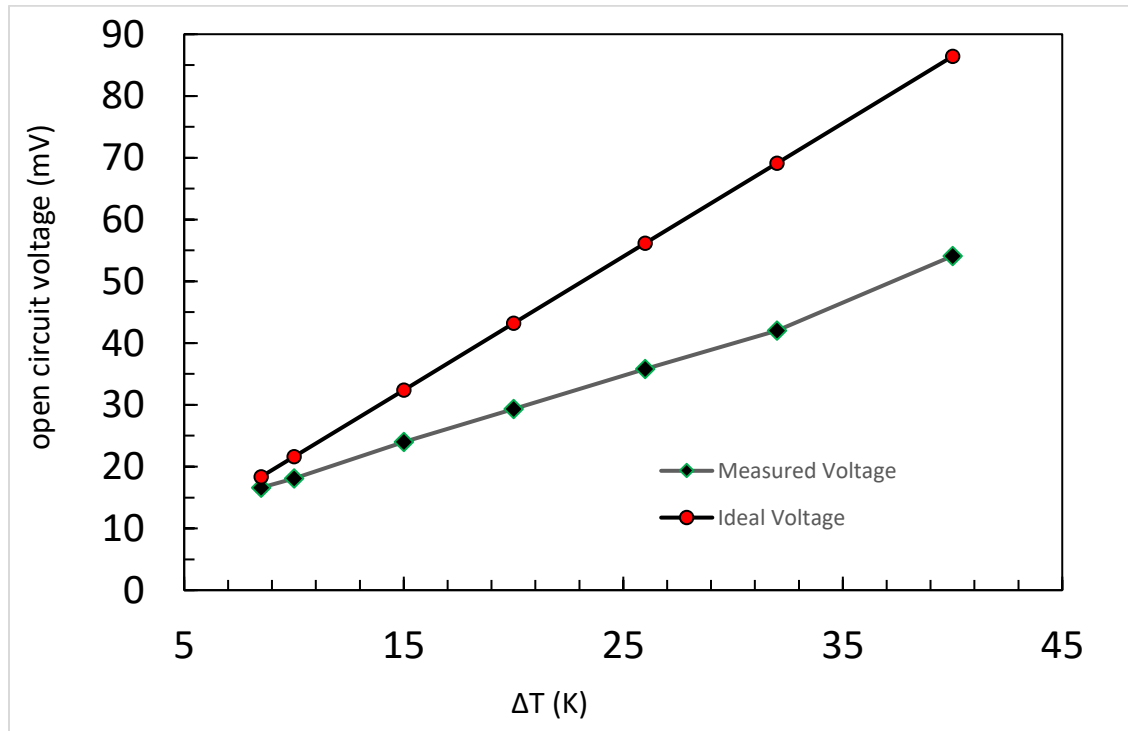


Fig. 6. Measured open circuit voltage V_{OC} of the TEG prototype and ideal calculated voltage vs temperature differences (ΔT)

The overall resistance of the 9 couple (p-type chitosan-100 mesh BST and n-type chitosan-100 mesh Bi composite thermoelement) TEG prototype was 12Ω at room temperature. The output voltage was measured at specific temperature differences (10 K, 20 K, and 40 K) and at various load resistances. Fig. 7 shows the voltage and power output versus current at ΔT of 10 K, 20 K, and 40 K. As the current increased, the voltage output decreased. On the other hand, the power output of TEG first increases and reaches maximum value and then starts decreasing followed a parabolic function based on Eq. (2). The maximum power output of TEG prototype was obtained

when the external load resistance matches the TEG device resistance. At this point, the closed-circuit voltage value was approximately half of the value of the open circuit voltage. At ΔT of 40 K, the TEG prototype produced a maximum power output of 73 μW while the close circuit voltage was 26 mV, and the current was 2.8 mA.

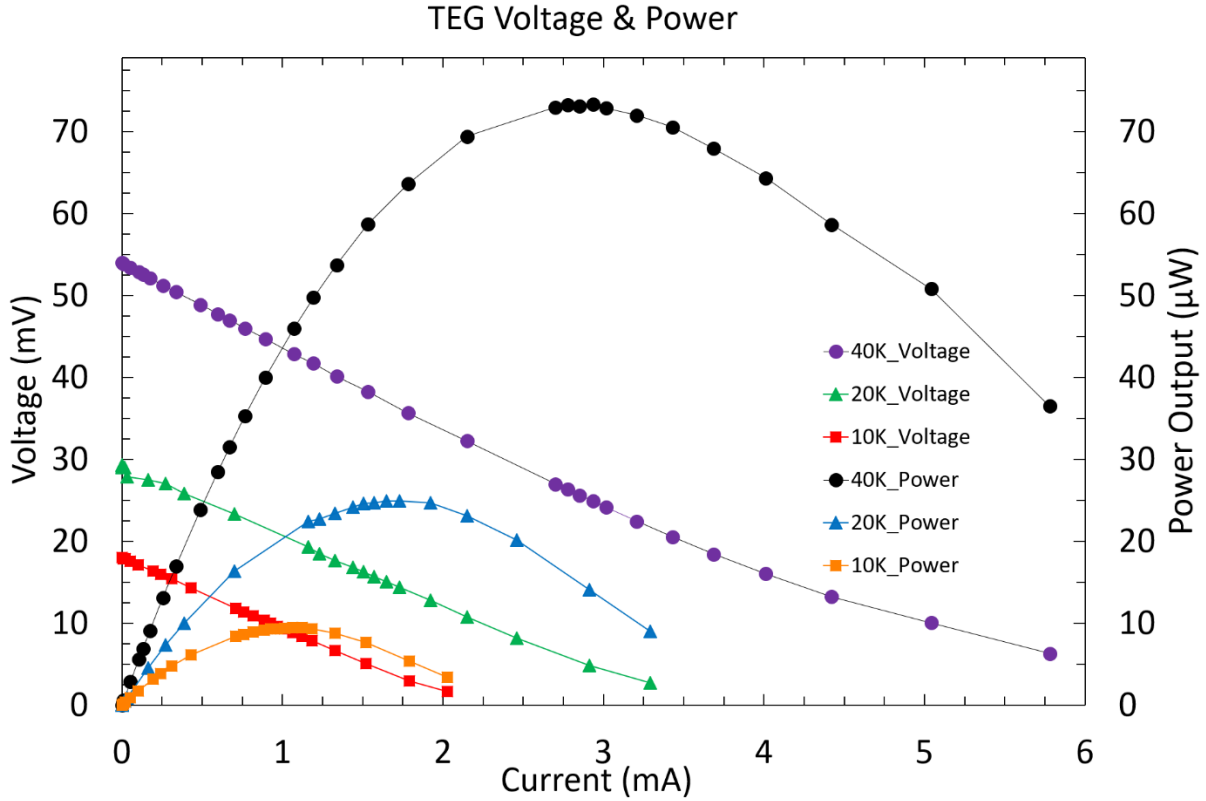


Fig. 7. Voltage and power output as a function of current at various ΔT (10 K, 20 K, and 40 K)

Fig. 8 shows the measured power density (measured power output of TEG device per unit cross-sectional area of the TEG device) of actual prototype and fitted model power density of the TEG prototype using Eq. (2,3,4) as a function of the temperature differences. The power density of the fitted model was calculated by using the TEG prototype device resistance (12Ω), the calculated open circuit voltage used in Eq. (1) and the cross-sectional area of the TEG prototype A_{TEG} using Eq (3).

$$P = \frac{[m(\alpha_n + \alpha_p)\Delta T]^2}{4R_{TEG}} \quad (2)$$

Here, m , α_n , α_p , and ΔT have already been defined in the paragraph above while R_{TEG} , is the resistance of the TEG device (12Ω). The total cross-sectional area of the TEG prototype is given below.

$$A_{TEG} = 2m(A_0 + A_s) \quad (3)$$

Here, A_0 = width of thermoelement (2.3 mm) × thickness (150 μm)

and, A_s = spacing between two thermoelements (2.5 mm) × thickness (150 μm)

The equation for the calculation of power density is

$$PD = \frac{P}{A_{TEG}} \quad (4)$$

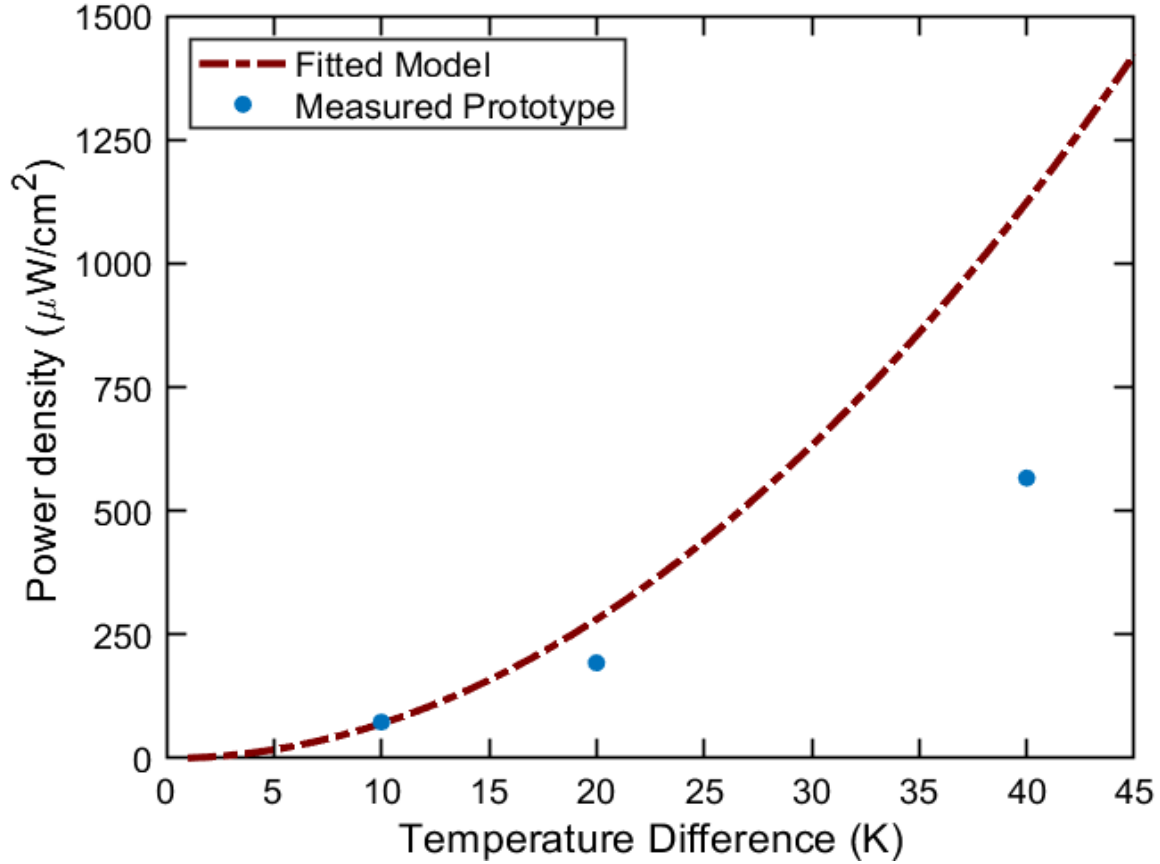


Fig. 8. Power density as a function of temperature difference for measured prototype (blue dots), fitted model (brown line)

From Fig. 8, it is quite evident that the measured power output and power density values for the TEG prototype device are close to fitted model at ΔT of 10 K, 20 K. However, as the temperature difference increases, the measured power density of actual prototype approaches towards a much lower value than the power density obtained from the fitted model. In the case of fitted model, as mentioned above, we used the device resistance (12 Ω) and calculated the voltage based on the Seebeck coefficient of n and p-type composite films, finally to calculate the power of fitted model. Therefore, we can say that measured voltage output of TEG device was very close to the calculated voltage of TEG device at lower ΔT of 10 K and 20 K. At ΔT of 40 K, however, as we discussed in the case of open circuit voltage shown in Fig. 6, it becomes difficult to maintain a high ΔT across the TEG prototype. Therefore, we observed that the measured output voltage

of TEG device at ΔT of 40 K was much less (54 mV) than the calculated open circuit voltage (85 mV). Moreover, the open circuit voltage is linearly proportional to ΔT , however, the power output is proportional to the square of ΔT as can be seen from equation (2). Thus, as ΔT increases the measured power output (73 μW) of TEG device deviates from the fitted model (145 μW). And, therefore, the power density of actual prototype (566 $\mu\text{W}/\text{cm}^2$) was lower as compare to fitted model (1123 $\mu\text{W}/\text{cm}^2$) at ΔT of 40 K [5,12,18]. Moreover, at high temperature, we have observed a change in resistance of the device which also contributes to lower power density (566 $\mu\text{W}/\text{cm}^2$) at ΔT of 40 K as compared to fitted model (1123 $\mu\text{W}/\text{cm}^2$).

The voltage and power output characterization of the TEG prototype was carried out again after 100 days since the first measurement. The purpose of this second measurement was to find out the stability and reliability of the prototype in open air atmosphere. During the second measurement, the prototype's resistance and the open-circuit voltage were measured, and the maximum power output was calculated based on the measured voltage and the external load resistance. After 100 days, we noticed that the TEG prototype resistance increased from 12 Ω to 16 Ω and the open circuit voltage increased from 54 mV to 59 mV at a ΔT of 40 K. This resistance and voltage values of prototype device shows a slight increase from previous measurements which could be due to multiple bending, mishandling, movement caused due to changing locations and leaving device in open air atmosphere. The maximum power output of TEG prototype was recorded to be 66 μW for a voltage of 27.2 mV and current of 2.4 mA at a ΔT of 40 K as shown in Fig 9. The maximum power output (66 μW) of TEG after 100 days of measurements was 10% less than the original measurement of TEG prototype (73 μW). Therefore, based on these results we can say that the thermoelectric prototype fabricated in this study is relatively stable and reliable in the open-air atmosphere.

Table 1 shows the comparison between the power output and power density of various printable TEGs devices reported in the literature as well as in our work. The first three TEG devices in the table are epoxy binder-inorganic thermoelectric composite dispenser printed TEGs on gold coated polyimide substrate [5,12,34]. For epoxy Bi-BST 10-couple dispenser printed TEG circular device, maximum open circuit voltage of 230 mV was achieved at a ΔT of 70 K. The maximum power reported at this ΔT was 130 μW while the power density was 1230 $\mu\text{W}/\text{cm}^2$ [34]. To cure the epoxy binder in thermoelectric composite films and sinter the thermoelectric particles so as to decrease the grain boundaries and enhance the electrical conductivity, a long duration of curing (6-12 hours) at a high temperature (250-350 $^{\circ}\text{C}$) was required (high energy- intensive curing process). Cho et al fabricated a flexible 3D screen printed device and achieved the maximum voltage of 850 mV, the maximum power of 310 mW, and the power density of 7.3 mW/cm^2 at ΔT of 28 K for 200 thermoelectric couples [9]. To fabricate the screen printed flexible TEG, this group used thermoelectric inorganic materials with a removable binder, the highest power output and power density results are mentioned in Table 1. To remove the binder and sinter the particles to make continuous films, they used high temperature sintering with temperature ranging up to 500 $^{\circ}\text{C}$ and the duration of curing spanning up to 6 hours. Varghese et al. recently fabricated a four p-element planar TEG and reported a power output of 54 μW and power density of 18.8 mW/cm^2 at ΔT of 80 K as shown in the Table 1 [18]. They used tellurium nanoparticles to fill the gaps between the BST particles and removable binder to enhance the electrical conductivity thus achieving a high-power factor (3 mW/mK^2) for the TE composite material. This group also used high temperature sintering with temperature ranging up to 450 $^{\circ}\text{C}$ and the duration of curing spanning up to 2.5

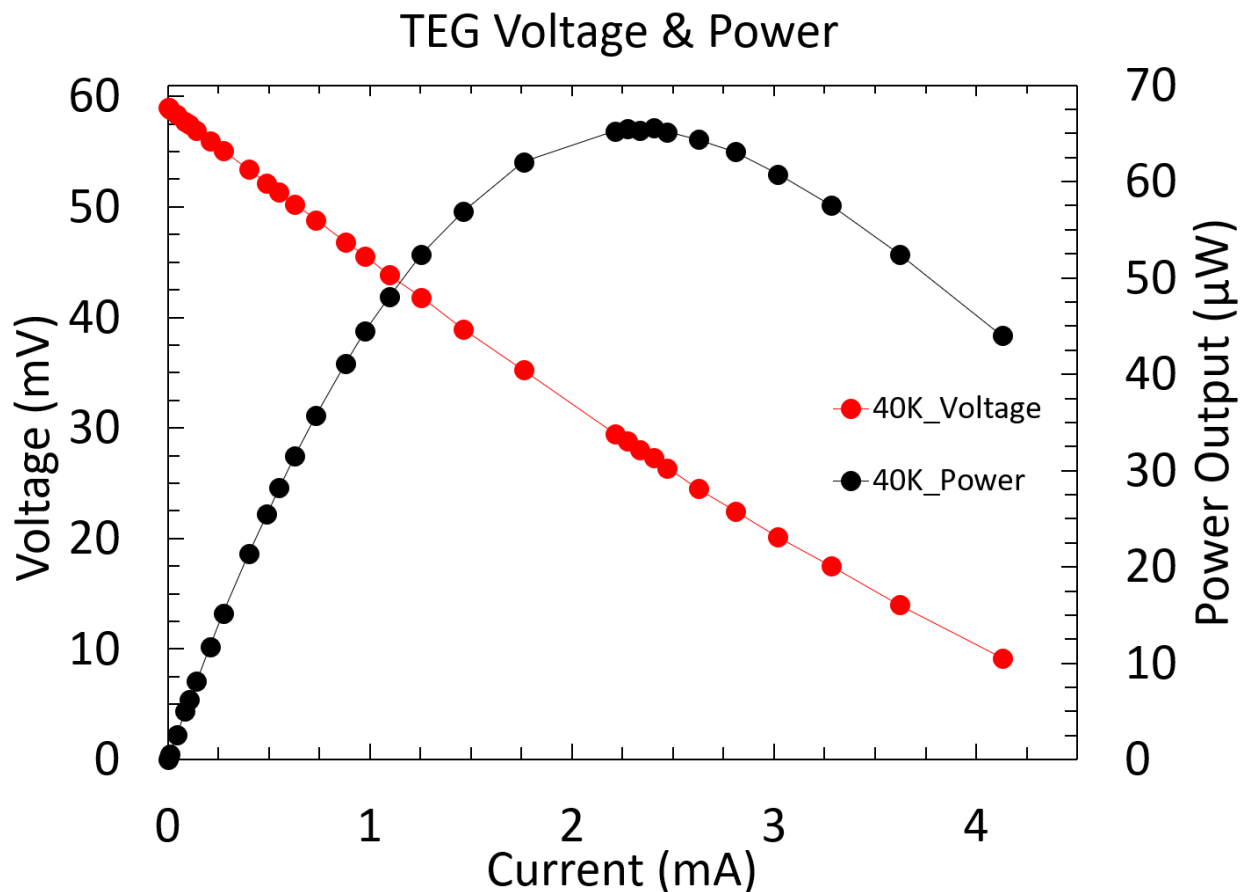


Fig. 9. Voltage and power output of the TEG prototype measured after 100 days

hours to achieve a high-power factor and high-power density as mentioned in Table1. Cao et al. successfully fabricated a flexible TEG prototype consisting of 8 thermocouples using screen-printing method. An epoxy binder was used to provide sufficient adhesive properties to the TE particles. Like all the aforementioned groups, this group also used a high temperature curing ranging up to 250 °C and the duration of curing spanning up to 3 hours [19,20]. It is encouraging to know that the prototype fabricated using naturally occurring materials and an energy-efficient method has a power output and power density comparable to the other printable TEG devices which were fabricated using energy-intensive methods as shown in table1.

Using mostly naturally available materials (Bi and chitosan), energy efficient methods for curing (small amount of binder, utilizing heterogeneous distribution of thermoelectric particles, low temperature curing (120°C for 30 minutes) and pressing at 200 MPa) and cost-effective screen-printing technique, these TEG devices can be easily produced at a large-scale. Thus, contributing to the reduction of the cost per unit area of the fabricated TEGs and helping in achieving the goal of mass production of TEGs. These TEG devices are easy to stencil print on a large scale. It is also quite easy to change the aspect ratio of these device and increase the number of couples to make them suitable for specific applications by using various CAD modeling software and producing stencil masks of desired dimensions. The power and power density values obtained by the TEG prototype presented in this study will be sufficient to supply power to wireless sensors (10 μW ~ 1.8 mW) and wearable sensors (< 70μW). These TEG devices can be easily used in

various low-grade waste heat scavenging applications [5,35,36]. Since these TEG have been fabricated on Kevlar substrate, therefore, it can also be easily used for waste heat recovery applications on non-planar surfaces. Given the existing restrictions of rigid and flammable battery systems, the development of printable and scalable planar TEGs will provide a self-sufficient power solution to mitigate the power needs of wearable device technologies for the present and the future [5]. These TEGs can be integrated with rechargeable batteries to supply enough power to charge these batteries. This integrated system of TEG and rechargeable batteries would be very useful to power the WSN system (especially at remote location) for long period of time without worrying to replace the batteries frequently.

Table 1

Comparison of printed TEG device performances among various reported work and this study

Ref.	# of couples	Dimensions	Resistance	ΔT	Max. voltage	Max. Power	Power density	Max. curing Temp.	Max. curing Time
[12]	50	5 mm×640 μm ×90 μm	2.33 k Ω	20 K	171.6 mV	10.5 μW	75 $\mu\text{W}/\text{cm}^2$	523 K	>360 min
[34]	10	5 mm×1.5 mm×120 μm	100 Ω	70 K	230 mV	130 μW	1230 $\mu\text{W}/\text{cm}^2$	523 K	>360 min
[5]	5×10	3.5 mm×600 μm ×100 μm	55 Ω	20 K	88 mV	33 μW	280 $\mu\text{W}/\text{cm}^2$	523 K	>360 min
[9]	200	2 mmD×650 μm	1.49 Ω	28 K	850 mV	310 mW	7.34 mW/cm ²	773 K	~100min
[18]	4	10 mm×2.7 mm×27 μm	8.5 Ω	80 K	60 mV	54 μW	18.8 mW/cm ²	723 K	~136 min
[10]	8	15 mm×20 mm×500 μm	0.35 Ω	50 K	90 mV		3.8 mW/cm ²	803 K	>145 min
[4]	200	2 mm D×650 μm		25 K		220 mW	5.23 mW/cm ²	773 K	240-340 min
[19]	1	39.3 mm×3 mm×64.5 μm		20 K	6 mV	48 nW		523 K	>180 min
[20]	8	20 mm×2 mm×67 μm	592 Ω	20 K	32 mV	444 nW		523 K	>180 min
This work	9	6.5 mm×2.3 mm×150 μm	12 Ω	40 K	54 mV	73 μW	566 $\mu\text{W}/\text{cm}^2$	393 K	<60 min

Conclusion

In this work, a planar TEG made of 9 thermocouples was stencil printed using p-type chitosan-100 mesh BST (1:2000 wt. ratio) and n-type chitosan with naturally occurring 100 mesh Bi (1:2000 wt. ratio) composite inks. A naturally occurring chitosan binder was used in small amount which provide enough adhesion strength to hold thermoelectric particles together. The heterogenous distribution of thermoelectric particles with varying sizes was used which resulted in the formation of a compact and dense composite films/thermoelements. These composite films/thermoelements were cured using hot pressing, 120 °C for 30 minutes at 200 MPa. A 9 - couple TEG prototype constitutes of n and p-type thermoelectric elements (2.3 mm × 6 mm × 150 μm) was fabricated on a Kevlar substrate attached with a gold coated copper metal electrode. The TEG prototype generated a maximum power output of 73 μW at 2.9 mA current and a closed-circuit voltage of 25 mV at ΔT of 40 K. Also, a maximum areal power density of 566 $\mu\text{W}/\text{cm}^2$ was

obtained at ΔT of 40K. The power and power density generated from these costs effective, energy efficient and scalable TEGs are suitable for various low-grade waste heat recovery applications. Moreover, the power output and power density of the TEG prototype reported in this study is sufficient to power various WSN and wearable medical devices. Our group successfully achieved a high-power output and power density which is comparable to the best reported power output and density values by using an energy-efficient method (small amount of binder, heterogenous distribution of particle size, hot pressing at 120 °C for 30 minutes at 200 MPa, and printing). Moreover, the utilization of earth abundant materials like chitosan and bismuth, contributed to the reduction of the cost per unit area of the fabricated TEGs thereby helping to achieve the goal of mass production of TEGs.

Acknowledgements

The authors would like to acknowledge support from University of Maryland Baltimore County (UMBC) for supporting this research through start-up fund. The authors would also like to thank Preetham Gowni (High school student) , for creating the matlab program for automation of device testing setup.

References

- [1] Akhtar F, Rehmani MH. Energy replenishment using renewable and traditional energy resources for sustainable wireless sensor networks: A review. *Renew. Sustain Energy Rev* 2015;45: 769–784.
- [2] Guan M, Wang K, Xu D, Liao WH. Design and experimental investigation of a low-voltage thermoelectric energy harvesting system for wireless sensor nodes. *Energy Convers Manag* 2017;138:30–37.
- [3] Hamid Elsheikh M, Shnawah DA, Sabri MFM, Said SBM, Haji Hasan M, Ali Bashir MB, Mohamad M. A review on thermoelectric renewable energy: Principle parameters that affect their performance. *Renew Sustain Energy Rev* 2014;30:337–355.
- [4] Choi H, Kim YJ, Kim CS, Yang HM, Oh MW, Cho BJ. Enhancement of reproducibility and reliability in a high-performance flexible thermoelectric generator using screen-printed materials. *Nano Energy* 2018;46:39–44.
- [5] Madan D, Wang Z, Wright PK, Evans JW. Printed flexible thermoelectric generators for use on low levels of waste heat. *Appl Energy* 2015;156:587–592.
- [6] Glatz W, Muntwyler S, Hierold C. Optimization and fabrication of thick flexible polymer based micro thermoelectric generator. *Sensors Actuators A Phys* 2006;132:337–345.
- [7] Park SH, Jo S, Kwon B, Kim F, Ban HW, Lee JE, et al. High-performance shape-engineerable thermoelectric painting, *Nat Commun* 2016; 7:1–10.
- [8] Park JW, Kim CS, Choi H, Kim YJ, Lee GS, Cho BJ, A Flexible Micro-Thermoelectric Generator Sticker with Trapezoidal-Shaped Legs for Large Temperature Gradient and High-Power Density, *Adv Mater Techno* 2020; 5 (10), 2000486.

- [9] Choi H, Kim SJ, Kim Y, We JH, Oh MW, Cho BJ. Enhanced thermoelectric properties of screen-printed $\text{Bi}_{0.5}\text{Sb}_{1.5}\text{Te}_3$ and $\text{Bi}_2\text{Te}_{2.7}\text{Se}_{0.3}$ thick films using a post annealing process with mechanical pressure. *J Mater Chem C* 2017;5:8559–8565.
- [10] Kim SJ, We JH, Cho BJ. A wearable thermoelectric generator fabricated on a glass fabric. *Energy Environ Sci* 2014;7:1959-1965.
- [11] Yuan Z, Tang X, Xu Z, Li J, Chen W, Liu K, et al. Screen-printed radial structure micro radioisotope thermoelectric generator, *Appl. Energy* 2018; 225,746–754.
- [12] Chen A, Madan D, Wright PK, Evans JW. Dispenser-printed planar thick-film thermoelectric energy generators. *J Micromechanics Microengineering* 2011;21:104006.
- [13] Madan D, Zhao X, Ireland RM, Katz HE. Conductivity and Power Factor Enhancement of n-type Semiconducting Polymers Using Sodium Silica Gel Dopant. *APL Mater* 2017: 5, 086106.
- [14] Byun SH, Kim CS, Agno KC, Lee S, Li Z, Cho BJ, et al. Design Strategy for Transformative Electronic System toward Rapid, Bidirectional Stiffness Tuning using Graphene and Flexible Thermoelectric Device Interfaces. *Adv. Mater* 2021: 33(10), 2170076.
- [15] Madan D, Chen A, Wright PK, Evans JW. Dispenser printed composite thermoelectric thick films for thermoelectric generator applications. *J Appl Phys* 2011;109:034904-034910.
- [16] Chen A, Madan D, Koplow M, Wright PK, Evans JW. Dispenser printed thermoelectric energy generators. *Proc PowerMEMS* 2009;277–280.
- [17] Madan D, Wang Z, Chen A, Juang R-C, Keis J, Wright PK, Evans JW. Enhanced performance of dispenser printed MA n-type Bi_2Te_3 composite thermoelectric generators. *ACS Appl Mater Interfaces* 2012;4:6117–6124.
- [18] Varghese T, Dun C, Kempf N, Saeidi-Javash M, Karthik C, Richardson J, Hollar C, Estrada D, Zhang Y. Flexible Thermoelectric Devices of Ultrahigh Power Factor by Scalable Printing and Interface Engineering. *Adv Funct Mater* 2019;1905796:1–8.
- [19] Cao Z, Koukharenko E, Tudor MJ, Torah RN, Beeby SP. Screen printed flexible Bi_2Te_3 - Sb_2Te_3 based thermoelectric generator. *J Phys Conf Ser* 2013;476:012031.
- [20] Cao Z, Koukharenko E, Tudor MJ, Torah RN, Beeby SP. Flexible screen printed thermoelectric generator with enhanced processes and materials. *Sens Actuators A: Phys* 2016;238:196–206.
- [21] Lu Z, Zhang H, Mao C, Li CM. Silk fabric-based wearable thermoelectric generator for energy harvesting from the human body *Appl Energy* 2016;164:57–63.
- [22] Kim SJ, We JH, Kim JS, Kim GS, Cho BJ. Thermoelectric properties of P-type Sb_2Te_3 thick film processed by a screen-printing technique and a subsequent annealing process.

J Alloys Compd 2014;582:177–180.

- [23] Madan D, Chen A, Wright PK, Evans JW. Printed Se-doped MA n-Type Bi_2Te_3 thick-film thermoelectric generators. J Electron Mater 2012; 41(6):1481–1486.
- [24] Jang E, Poosapati A, Jang N, Hu L, Duffy M, Zupan M, et al. Thermoelectric properties enhancement of p-type composite films using wood-based binder and mechanical pressing. Sci. Rep 2019; 9(1)7869.
- [25] Jang E, Possapati A, Madan D. Enhanced thermoelectric properties of F4TCNQ doped P3HT and its use as a binder for Sb_2Te_3 based printed thermoelectric films. ACS Appl Energy Mater 2018;1(4):1455–1462.
- [26] Huang J, Li H, Kirksey E, Hoffman C, Jang HJ, Wagner J, Madan D, Katz HE. Promising Thermoelectric Properties of Commercial PEDOT : PSS Materials and their Bi_2Te_3 Powder Composites. J Appl Phys 2019;125:125502.
- [27] Madan D, Wang Z, Chen A, Wright PK, Evans JW. High-Performance Dispenser Printed MA p-Type $\text{Bi}_{0.5}\text{Sb}_{1.5}\text{Te}_3$ Flexible Thermoelectric Generators for Powering Wireless Sensor Networks. ACS Appl Mater Interfaces 2013;5:11872–11876.
- [28] Varghese T, Hollar C, Richardson J, Kempf N, Han C, Gamarachchi P, Estrada D, Mehta RJ, Zhang Y. High-performance and flexible thermoelectric films by screen printing solution-processed nanoplate crystals. Sci Rep 2016;6:6–11.
- [29] Shin S, Kumar R, Roh JW, Ko DS, Kim HS, Kim SI, Yin L, Schlossberg SM, Cui S, You JM, Kwon S, Zheng J, Wang J, Chen R. High-Performance Screen-Printed Thermoelectric Films on Fabrics. Sci Rep 2017;7:1–9.
- [30] Jang E, Banerjee P, Huang J, Holley R, Gaskins JT, Hoque MSB, Hopkins PE, Madan D. Thermoelectric performance enhancement of naturally occurring Bi and chitosan composite films using energy efficient method. Electron 2020;9:1–12.
- [31] Banerjee P, Jang E, Huang J, Holley R, Vadrnala S, Sheikh A, et al. Thermoelectric Performance Enhancement of n-type Chitosan- $\text{Bi}_2\text{Te}_{2.7}\text{Se}_{0.3}$ Composite Films Using Heterogeneous Grains and Mechanical Pressure. J. Electron. Mater 2021.
- [32] Poudel B, Hao Q, Ma Y, Lan Y, Minnich A, Yu B, Yan X, Wang D, Muto A, Vashaee D, Chen X, Liu J, Dresselhaus MS, Chen G, Ren Z. High-thermoelectric performance of nanostructured bismuth antimony telluride bulk alloys. Science 2008;320:634–638.
- [33] Hostler SR, Qu YQ, Demko MT, Abramson AR, Qiu X, Burda C. Thermoelectric properties of pressed bismuth nanoparticles. Superlattices Microstruct 2008;43:195–207.
- [34] Madan D, Wang Z, Chen A, Winslow R, Wright PK, Evans JW. Dispenser printed circular thermoelectric devices using Bi and $\text{Bi}_{0.5}\text{Sb}_{1.5}\text{Te}_3$. Appl Phys Lett 2014;104:2012–2016.
- [35] Madan D. High Performance Dispenser Printed Thermoelectric Generators. University of California, Berkeley, 2013.

- [36] Chen A. Thermal Energy Harvesting with Thermoelectrics for Self-powered Sensors: With Applications to Implantable Medical Devices, Body Sensor Networks and Aging in Place. University of California, Berkeley, 2011.